Resonant soft x-ray scattering and charge density waves in correlated systems

Rusydi, Andrivo

Chapter 1

Introduction

1. 1. Strongly correlated system

The aim of condensed matter research is to understand the macroscopic behavior of systems, in all their rich diversity, starting from a detailed description of the individual particles and the way they interact. Almost a century ago, the history of strongly correlated electron systems began. In 1930's, Bloch [1] and Wilson [2] developed the band theory of solids. According to their band theory, a crystal is a metal if the highest energy occupied band is partially occupied and an insulator if this band is full. Band theory assumes that every electron is moving in a periodic potential created by the positive ions and by the average potential of the other electrons. In this one electron picture, every electron is sensitive only to the average properties of the surrounding environment, all correlations being neglected. The eigenstates of this one-particle problem, with the corresponding energies take on continuous values within distinct intervals, constituting the bands.

Although very successful in describing basic properties of many systems the perspective that this was a general theory did not last long. In 1937, de Boer and Verweij [3] pointed out that the Bloch and Wilson picture broke down for a large number of insulating 3*d* transition metal compounds, such as NiO and CoO, which were predicted to be metals. In fact, these materials are insulators with a conductivity gap an order of magnitude larger then the maximum gap derived even with the most sophisticated band structure calculation techniques. Mott and Peierls [4] were the first to suggest that the reason for the band theory failure might be the neglect of the repulsive Coulomb interaction between electrons on the *d* orbitals. Later on, Mott [5,6,7] and Hubbard [8,9] showed that if the repulsion is larger than the bare electron bandwidth the Fermi level will be located inside a gap and the system will be indeed an insulator. In the mean time, Anderson [10] introduced super-exchange in a model with a large *d*-*d* Coulomb interaction of local 3*d* electrons in competition with the energy lowering via hopping. This model is virtually identical to the Hubbard model.

In another class of phenomena, the Kondo [11] and heavy Fermion [12] phenomena, magnetic impurities in a metal or even a lattice of these magnetic "impurities" are considered, and also here the on-site Coulomb interaction "U" plays an important role.

Anderson [13] introduced the "Anderson Hamiltonian" to address these phenomena. The Coulomb interaction between the local *d* or *f* electrons in the magnetic impurity plays an important role and its strength relative to the hybridization-induced so-called virtual-bound-state broadening determines whether or not a local magnetic moments exist. In the large U limit, the Anderson Hamiltonian can be transformed to the low-energy-scale Kondo Hamiltonian [11], in which only the spin degrees of freedom of the impurities are retained.

The interaction of two electrons, which forms the basic part of these models, is rather simple. However, when many of these interacting particles are put together, i.e., when a two-body or three-body problem becomes a many body problem, correlation effects become dominant and account for a vast number of complex and often surprising phenomena. Arguably the biggest intellectual challenge in condensed matter physics to date is to obtain an understanding of the many body problem and its manifestation in a large variety of phenomena, which include the metal-insulator transition, insulator-superconductor transition, Kondo effects, heavy-fermion systems, high-temperature superconductors, mixed-valence systems, the quantum Hall effect, colossal magneto-resistance, charge ordering, and so on.

Although far from being solved, the strongly correlated system or many body problem can be described and studied at different levels of sophistication. In the 'ideal case', one needs to solve an exact Hamiltonian that includes all the Coulomb interactions between all the particles, in which it can be written as

$$H_{exact} = \sum_i \frac{\vec{p}_i^2}{2m_e} + \sum_{i,j} \frac{e^2}{|r_i - r_j|} + \sum_m \frac{\vec{P}_m^2}{2M_m} + \sum_{m,n} \frac{Z_m Z_n e^2}{|R_m - R_n|} + \sum_{i,m} \frac{Z_m e^2}{|R_m - r_i|} \qquad (1.1.1)$$

where all the variables follow the common conventions, in which the upper case letters represent ions and the lower case letters represent electrons. This "exact" (aside from relativistic effects) Hamiltonian, unfortunately is not solvable because the number of particles involved are of the order of 10^{23} per cubic centimeter.

An alternative procedure is to divide the system into parts, represent each part with effective parameters, and simplify the interaction between parts into the effective ones. By extracting the most important interactions and summing over the parts, one can build up an effective, relatively simpler model, which hopefully still accounts for the major collective properties of the system. It is widely accepted that it is more important to understand the low energy excursion from the ground state with energies of order *kT*. For example, in the Hubbard model for high temperature superconductors, each site is represented by one orbital which can be unoccupied, single occupied with either spin up or spin down or doubly occupied. Electrons in these orbitals have effective hopping integrals (*t*) to neighboring sites, and an effective on-site Coulomb repulsion (U) representing the correlation effects, which will be discussed later. This second approach is widely adopted and as a result, many models, such as Hubbard model, *t-J* model, and *t-t'-t"-J* model [14],

have been developed and many useful qualitative results have been obtained. Although analytic solutions are not available, except in special cases such as one dimension, these models provide the basis for many of the discussions.

Another approach based on the existing theories for weakly correlated or uncorrelated systems is the Fermi liquid theory. The extension of these theories, such as LDA (local density approximation in density functional approaches) [15,16], extended to LDA+U [17], various perturbation theories, marginal Fermi liquid (MFL) [18], near antiferromagnetic Fermi liquid (NAFL) [19], have been proposed to describe the strongly correlated system. In general, these theories can account for some aspects of the physics, but they fail to describe many other aspects of the system.

Beside the theoretical approaches, one can also follow a more conceptual and qualitative approach as an experimentalist might do. The major task of an experimentalist is to discover new phenomena, measure the properties of interesting materials and provide experimental tests of theoretical predictions. Since no one theory in fields involving correlated electron systems is generally accepted, no paradigm is available, and we should not be too surprised that new phenomena can be discovered. It is common that an experimentalist builds “gedanken” experiment based on an existing concepts and phenomena. During the experiment, one is aware that the model is simply a conceptualization, and one searches for traces of interesting physics in the data.

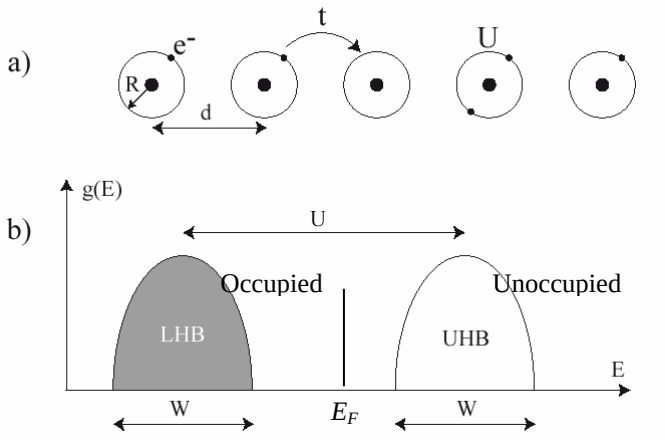

Figure 1.1.1 (**a**) one dimensional hydrogen chain. R denotes the radius of a 1*s* Bohr orbit, d is the interatomic spacing (**b**) Density of state for half filled one band Hubbard model for U>W. In one dimension W = 4t and in two-dimensional W = 8t for a square lattice.

Let's go back to the theoretical approach. A simple and yet physically reliable model to describe electron correlation is the one-band Hubbard model where the Hamiltonian is given by

$$H = -\sum_{i,\sigma} t_{i,i+1}\left(c^{+}_{i,\sigma}c_{i+1,\sigma} + c^{+}_{i+1,\sigma}c_{i,\sigma}\right) + \sum_{i} U\, n_{i,\sigma}n_{i,-\sigma} \qquad (1.1.2)$$

where t and U are the intersite one-electron transfer integral and the on-site Coulomb repulsion, respectively. $c^{+}_{i\sigma}$ creates an electron with spin σ at lattice site-i and and $n_{i\sigma}$ is the number operator for an electron at site i with spin σ. t delocalizes the electrons over chain while U keeps the electrons apart. The ratio U/t is an important parameter for magnetic and electrical properties. For U<<t, a simple tight binding energy is obtained with an enhanced magnetic susceptibility [20]. For U>>t or large, a strongly correlated metal or Mott-Hubbard insulator is found with linear Heisenberg antiferromagnetic behavior [21].

Consider a one dimensional hydrogen chain as shown in **Fig. 1.1.1**(**a**). The first term of eq. (1.1.2) is the kinetic energy, where t_{ij} = 0 unless the ith and jth sites are nearest neighbors. U is the on-site Coulomb repulsion between electrons. This model does not account for long-range Coulomb repulsion, multi-band effects, orbital degeneracy etc., but it does describe how a half-filled band splits into an empty upper Hubbard band (UHB) and a filled lower Hubbard band (LHB). When the band width W=4t is smaller than U, there is a gap between the occupied and unoccupied states and the system becomes a Mott insulator [see **Fig. 1.1.1**(**b**)]. Let's consider two extreme types of valence states. When the orbital radius R (determines U) is much larger than the distance between sites d (R/d determines t), or in other words large overlap between orbitals on neighboring sites then one would expect that: (1) the valence orbitals have lost their atomic identity, (2) the energy dispersion $\varepsilon(k)$(where k is the wave vector) is large, (3) small electron-electron interaction (U<<W), (4) the system is metallic with low energy scale charge fluctuations and (5) the system is non-magnetic because each Bloch state will be occupied by two electrons one of each spin direction. When d >> R, then one would expect that: (1) the valence orbitals remain atomic-like, (2) the energy dispersion $\varepsilon(k)$ is small, (3) strong electron-electron interaction (U>>W), (4) there is a large gap for charge fluctuations, (5) each state is single occupied leading to local spins, and (6) the low energy scale is dominated by spin fluctuations. The condition of d >> R is believed to be responsible for physical and chemical properties of many transition metal oxides (3d) such as metals in CrO_2, Fe_3O_4, insulator in Cr_2O_3, CoO, V_2O_5, Co_3O_4, semiconductor to metal transition in VO_2, V_2O_3, Ti_4O_7, Superconductivity in $La_{2-x}Ba_xCuO_4$, $LiTiO_2$, piezoelectricity in $BaTiO_3$, CuCl, ferromagnetism in CrO_2, antiferromagnetism in MnO, ferrimagnetism in γFe_2O_3, etc.

As we said above, when the band width W is smaller than U, the system becomes a so-called Mott insulator [**Fig. 1.1.1**(**b**)]. A Mott insulator is a result of the competition between localization effects (on-site Coulomb interaction) and delocalization effects

(hopping to lower the kinetic energy). If t << U, where the on-site Coulomb interaction dominates, the energy gained by the delocalization of the electron is smaller than the cost of double occupancy, that is, the bandwidth W is smaller than U, the system will be insulating, and vice versa. Localization and delocalization are two very useful concepts in many-body physics. For example, in the case of rare earths, 4*f* orbitals are very localized, which correlates with the strong on-site Coulomb interactions in these systems. These account for the heavy Fermion systems and Kondo effects observed in lanthanide systems. For materials containing 3*d* transition metal elements, the strength of these two effects are comparable. Hybridization between the 3*d* orbital and the ligand atoms (e.g. O) is just as important. These systems exhibit extremely rich phenomena, such as high temperature superconductivity and colossal magneto-resistance.

In the infinite U limit of the *t-J* model, one gets another widely used model: the Heisenberg model. The large U forbids double occupancy and the effect of the on-site Coulomb interaction is to generate a nearest neighbor super exchange interaction J ($\sim t^2/U$), the magnetic exchange coupling between spins at neighboring sites. Similarly, in an extended version such as the *t-t'-t"-J* model, the hopping to next and next-next nearest neighbors are included.

Another factor, dimensionality, plays an important role in understanding the strongly correlated systems. In the *t-J* model, with J > 0, an antiferromagnetic ground state can be achieved in the classic limit. However, in the case of the two-dimensional S = 1/2 system, as Brinkman & Rice argued that the fluctuations could destroy the long range antiferromagnetic order, and a new type of ground state, namely the Resonance Valence Bond (RVB) state may appear [22] while Anderson suggested that the RVB state might cause High Tc [23]. This state has not been observed in experiments, but the basic idea it represents is widely used [24].

Speaking of dimensionality and the energy gain to have antiferromagnetic interaction, it is interesting to compare the classical Neel order mechanism versus the singlet liquid or RVB model. Denoting the magnetic sites by $\uparrow$ or $\downarrow$, the Neel order mechanism in two dimensional can be drawn as

$$\begin{array}{cccccccc} \uparrow & \downarrow & \uparrow & \downarrow & \uparrow & \downarrow & \uparrow & \downarrow \\ \downarrow & \uparrow & \downarrow & \uparrow & \downarrow & \uparrow & \downarrow & \uparrow \\ \uparrow & \downarrow & \uparrow & \downarrow & \uparrow & \downarrow & \uparrow & \downarrow \\ \downarrow & \uparrow & \downarrow & \uparrow & \downarrow & \uparrow & \downarrow & \uparrow \end{array}$$

The total spin for this condition is 0 while the local spin is ½ this would lead to a ground state energy in mean field theory of $E_{Neel} = -(J/4)(NZ/2)$, where Z is number of nearest neighbors. While for the singlet liquids or RVB mechanism, the energy where the total and

local spin are 0 is $E_{RVB} = -(N/2)(3J/4)$. It is clear that for $Z < 3$ such as in a one dimensional systems, the singlet liquid or RVB mechanism wins. In two dimensions, with Z = 4 things are less clear but we should realize that in less than half filled systems such as in the doped cuprates Z will be 3 or even less for some sites.

Charge-transfer and Mott-Hubbard insulators

In 1985, Zaanen-Sawatzky-Allen (ZSA) proposed a more general phase diagram for the transition metal oxides [25]. In their model, the direct overlap between the transition metal (TM) 3*d*-states can be neglected and consequently the electron hopping occurs not directly between the TM 3*d*-states but via the 2*p*-state of oxygen ligands. The hoping via the oxygen sites can be taken in-to account by the Hamiltonian

$$\begin{aligned} H = t_{pd} \sum_{\langle i,j\rangle,\sigma} \left(d_{i\sigma}^{+} p_{j\sigma} + h.c \right) + \varepsilon_d \sum_i d_{i\sigma}^{+} d_{i\sigma} + \varepsilon_p \sum_i p_{i\sigma}^{+} p_{i\sigma} \\ + U_{dd} \sum_i n_{i\uparrow}^{d} n_{i\downarrow}^{d} + U_{pp} \sum_i n_{i\uparrow}^{p} n_{i\downarrow}^{p} + V_{dp} \sum_{i,\sigma} n_{i\sigma}^{d} n_{i\sigma}^{p} \end{aligned} \tag{1.1.3}$$

where the transfer integral t_{pd} corresponds to the hopping between TM 3*d* and O 2*p*, ε_d (ε_p) is the atomic energy of a *d*-electron (*p*-electron), U_{dd} (U_{pp}) describes the onsite Coulomb repulsion between the *d*-electron (*p*-electron), and V_{dp} parameterizes the interaction between the *p*- and the *d*-states. The operators $d_{i\sigma}^{+}$ and $p_{i\sigma}^{+}$ create a *d*- and a *p*-electron with spin $\sigma = \uparrow,\downarrow$ at the lattice site i, respectively. And $n_{i\sigma}^{d}$ and $n_{i\sigma}^{p}$ are the number operators for *d*- and *p*-electrons.

A charge transfer is defined as $\Delta = \varepsilon_d - \varepsilon_p$. Depending on the ratio of Δ / U, the system can be classified as follows: If the energy of the 2*p* states is low enough (Δ > U), the low energy excitation is $d^n d^n \rightarrow d^{n-1} d^{n+1}$, i.e. the charge transfer from one TM site to another. In this case the low energy physics does not explicitly involve the oxygen *p*-state [see **Fig. 1.1.2**(**a**)]. The *p*-states only enter the effective hopping amplitude $t = t_{pd}/\Delta$ and the system can be described by the Hamiltonian given in eq. (1.1.2) Therefore, the condition U>>*t*, implies an antiferromagnetic insulating behavior. This class of systems is called Mott-Hubbard insulators. On the other hand, if Δ < U which is called a charge-transfer insulator, the low energy charge excitations correspond to a charge transfer from the oxygen to the TM 3*d* site [see **Fig. 1.1.2**(**b**)], which can be written as $p^6 d^n \rightarrow p^5 d^{n+1} = d^{n+1}\underline{L}$.

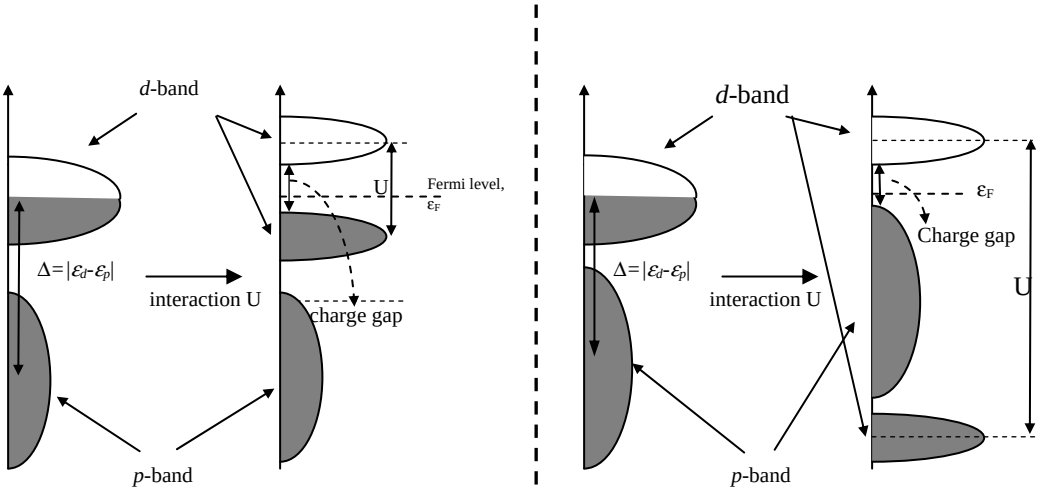

(**a**) Mott-Hubbard Insulator (**b**) Charge-Transfer Insulator

Figure 1.1.2 (**a**) Schematic band structure of a Mott Hubbard insulator. The *p*-band lies before the *d*-band, and the low energy charge excitations occur between the lower and upper Hubbard band. (**b**) Schematic band structure of a Charge-Transfer insulator. The *p*-band lies between the lower and upper Hubbard band. The lower energy charge excitation involves the *d* and *p*-bands.

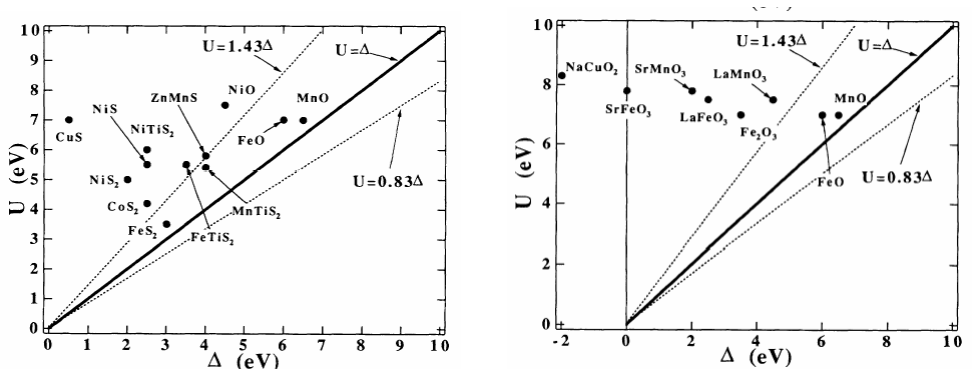

Figure 1.1.3 Zaanen-Sawatzky Allen Δ–U diagram for (**a**) divalent and (**b**) higher valent transition metal compounds study by ref. [26]. The regime above the line U=Δ is the charge trasfer regime while the regime below this line is the Mott-Hubbard regime.

It is important to note here that although the magnetic interaction of the charge-transfer insulator with n = 1 (one electron per site) and t <<Δ << U are very similar to the exchange interaction in an one-band Mott-Hubbard insulator the excitation spectra and charge transport can be different for the two material classes. In **Fig. 1.1.3** Zaanen-Sawatzky-Allen Δ–U diagram for (**a**) divalent and (**b**) higher valent transition metal compounds reported in ref. 26 is presented. A large number of compounds are situated near the phase boundary between the Mott-Hubbard and charge transfer regime. One can see that the CuO-system belongs to the charge-transfer insulator regime, i.e. the doped holes will be situated at the oxygen sites.

1. 2. High-temperature superconductors

In 1986 Bednorz and Müler [27] discovered a new type superconductor, based on Cu and O, with a critical temperature is about 30 K. Their discovery has been one of the most important discoveries in condensed matter physics of the second half of the last century. Soon after their discovery, a large number of similar materials (generically called "cuprates") were synthesized, having critical temperatures above the boiling point of liquid nitrogen (77 K) and therefore opening enormous opportunities for technological applications. The common belief is that the understanding of these materials could provide the knowledge for growing room temperature superconductors. Thus, since their discovery, the cuprates have been under an extraordinary intensive, both experimental and theoretical, investigation.

After more than 20 years of research, the cuprates are far from understood. As part of the puzzle of strongly correlated systems, they exhibit many "anomalous" properties, imposing severe constraints on any reasonable theory.

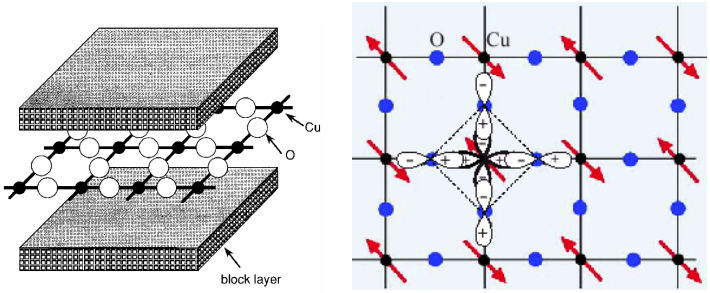

(**a**) (**b**)

Figure 1.2.1 (**a**) Conceptual illustration of staking of CuO_2 layers sandwiched by block layers. (**b**) Schematic of CuO_2 plane.

Despite their different chemical composition, the cuprate superconductors have many common characteristics, and it is natural to assume that these characteristics determine the basics physics. The high-T_c superconductors are layered materials, containing quasi-two-dimensional CuO_2 planes sandwiched between block layers. The generic structure is illustrated in **Fig. 1.2.1**, but it also should be said that some materials have more than one CuO_2 layer in between the block layers.

The electronic states close to the Fermi level are contained in the CuO_2 planes. The block layers play the role of charge reservoirs, controlling the number of charge carries in the conduction planes upon chemical doping. Consequently, theoretical models designed to describe the physics of a single CuO_2 plane for different electronic concentrations were proposed for the cuprates. However, there is no general agreement on what should be the minimal model that captures the basic physics of a CuO_2 plane.

The x-ray absorption (XAS) experiments show that the first electron addition states have O*p* origin, placing the cuprates in the charge-transfer regime of the ZSA-scheme [10] as we explained above. It is believed that the only Cu orbital which participates in the low-energy physics is the $d_{x^2-y^2}$ one. It couples to the in-plane oxygen *p* orbitals, and therefore the first models contained all these degrees of freedom (*d* and *p*). However, based on the strong Cu-O hybridization, many physicists believe that one step further can be taken and a reduction to a one-band Hamiltonian which contains only the $d_{x^2-y^2}$ orbitals can be made. But there is no general agreement for that and some authors consider the oxygen orbitals as essential for explaining the properties of the phase diagram, such as the pseudogap for example [28,29]. If the system is doped the added holes are believed to mainly occupy the Oxygen sites. In particular, Zhang and Rice [30] proposed that Cu-O hybridization strongly binds a hole on each square of O atoms to the central Cu 2^+ ion to form a local singlet, which is a coherent superposition of the $2p_\sigma$ orbitals of the four nearest-neighbour oxygen atoms [see **Fig. 1.2.1**(**b**)]. This so-called Zhang-Rice singlet moves through the lattice in a similar way as a hole in the single- band effective Hamiltonian of the strongly interacting Hubbard model, and has been used as the building block in the construction of an effective microscopic Hamiltonian for the cuprates. Because the low energy excitation is mainly the Zhang-Rice-Singlet band, it is also called the effective LHB in the literature.

The common physical properties of cuprates can be summarized in the generic phase diagram presented in **Fig. 1.2.2** [35]. The undoped materials are antiferromagnetic insulators. Upon doping the antiferromagnetism is quickly destroyed. For the doping range approximately in between 5% and 30%, the cuprates become superconductors at low temperature. The doping value where Tc is maximum (around 15%) is called optimal doping. The lower and higher doping regime are respectively called the underdoped and overdoped regimes. Unlike in conventional superconductors, the superconducting gap in

the cuprates has d-wave symmetry, with nodes along the diagonal directions and a sign change on a $\pi/2$ rotation [31,32,33,34]. In the overdoped region, above T_c the system is a Fermi-liquid metal. But the most intriguing physics occurs in the underdoped region, in the proximity of the antiferromagnetic phase. The majority of physicists believe that the understanding of the underdoped normal state would provide the key for elucidating the mechanism of superconductivity.

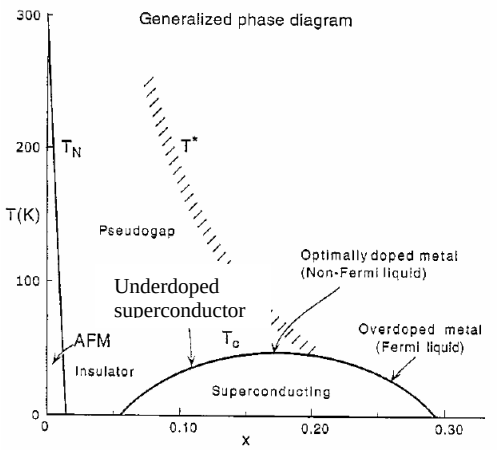

Figure 1.2.2 Generic phase diagram of doped hole cuprates superconductors [35].

1.3. Hole crystallization in Cu-O systems

As we discussed above, the character of the ground state of an antiferromagnetic insulator is fundamentally altered following addition of even a small amount of charge or holes [see **Fig. 1.2.2**]. At present, in the two-dimensional or quasi 2-dimensional Cu-O system, it is unclear whether the interaction between the doped holes is driven by the short-range exchange interaction, the long-range Coulomb interaction, or a combination of both. However, in the following we introduce briefly and focus our study on some of the most important ideas and scenarios which have appeared since the high T_c discovery. And so far, there is no direct experimental evidence that favors any of the scenarios.

The most often used model Hamiltonian is a 3-band Hubbard charge-transfer model as described by Zaanen-Sawatzky-Allen [25]. This model leads to an effective one-band Hubbard Hamiltonian with effective *U*, *t*, *t*' and *t*''. For large U it goes to *t*, *t*', *t*'' and *J* in which the neighboring spins are coupled via *J* and the hopping is controlled by the *t*'s. In all these models the long-range coulomb interaction is neglected and there is really no direct evidence that this is correct. For example if one has an effective attractive-nearest neighbor interaction as suggested in many models because of exchange of magnetic

fluctuations or phonons, etc, then one would perhaps expect phase separation into high density and low density regions if one neglects the long range coulomb interactions.

In two-dimensional Cu-O systems one of the candidate ground states, which has been proposed to compete with superconductivity, is the so called “stripe” phase. The stripe phase was proposed in terms of the electronic liquid-crystal of electron “nematic” model [36,38,39,40,41,41]. The added charge is concentrated in domain walls across which a phase shift by π in the spin correlations of the host material is induced. These domain walls are stripes which can be insulating [37,38] or conducting [39,40,41] —that is, metallic ‘rivers’ with their own low-energy degrees of freedom. However, in arrays of one-dimensional metals, which occur in materials such as organic conductors [42], interactions between stripes typically drive a transition to an insulating ordered charge-density-wave (CDW) state at low temperatures. Here, the CDW is a $4k_F$ CDW or Wigner Crystal (WC). As proposed by Kivelson *et. al.* [43] such a transition is eliminated if the zero-point energy of transverse stripe fluctuations is sufficiently large compared to the CDW coupling between stripes. As a consequence, there should exist electronic quantum liquid-crystal phases, which constitute new states of matter, and which can be either high-temperature superconductors or two-dimensional anisotropic ‘metallic’ non-Fermi liquids.

Another interaction which is also neglected is the long-range Coulomb interaction in theories based on resonating valence bond (RVB) and spin-charge separation [44,45]. Here the spins pair into short-ranged singlets, when $T < T^*$, resulting in a gap in the spin excitation spectrum which may be related to the pseudogap. The elementary excitations are not quasiparticles but spinons which are charge-neutral fermions with spin 1/2 and holons which are charged bosons with spin 0. At T_c the holons condense and recombine with the spinons giving rise to superconductivity.

On the other hand, Noda and Imada [46] studied the importance of the interplay of lattice commensurability and long-range Coulomb interactions for quantum phase transitions to charge-ordered and Wigner-crystal states in two-dimensional (2D) electron systems by quantum Monte Carlo calculations. In their study, they found another crucial concept, which is lattice commensurability which generates another dramatic effect of the periodic potential when the long-range Coulomb interaction is present.

Experimental evidence for such long-range order can be obtained with X-ray or Neutron Scattering. So far, the main experimental evidence for stripes in copper-oxides is neutron scattering from $La_{1.48}Nd_{0.4}Sr_{0.12}CuO_4$ [47] (LNSCO) and $La_{1.875}Ba_{0.125}CuO_4$ [48] (LBCO) which reveal coexisting static spin and charge order. Further, all such charge scattering is weak since a neutron is electrically neutral and detects only distortions in the crystal structure [49]. It is therefore not known whether the “stripe” phase in LNSCO and LBCO actually involves ordering of the doped holes. Interestingly, the charge/spin texture that develops in LNSCO and LBCO is visible only in the low temperature tetragonal (LTT) phase, is most stable at $x = 1/8$ and coincides with an anomalous suppression of T_c [50].

It is important to note here that the concept of stripe correlations does not by itself offer an explanation for superconductivity in the layered cuprates. But it does represent a new paradigm for the understanding of the electronic correlations in the normal state.

In quasi-two-dimensional Cu-O systems, the existence of hole crystallization was also studied intensively, starting from 1992 when Dagotto *et al.* [51] proposed an electronic model for ladder like structures in which the Copper and Oxygen ions are ordered in two parallel *t* - *J* chains forming the legs of a ladder and *t*'-*J*' coupling along the rungs. In their model, a pair of holes should exist along the rung, and depending upon the parameters chosen, a doped ladder can exhibit either exchange-driven superconductivity [51,52] or an insulating "hole crystal" ground state in which the carriers crystallize into a static, Wigner lattice [51,53,54]. Moreover, a recent calculation by White *et. al.* [54], using the DMRG method, the CDW is also a WC and it is stabilized at a filling of $n = 3/4$. The competition between these two phases is similar to that believed to occur between ordered stripes and superconductivity in two-dimensional Cu-O systems.

The only known doped ladder material is $Sr_{14-x}Ca_xCu_{24}O_{41}$ (SCCO). Superconductivity has indeed been found by Uehera *et al*. in $Sr_{0.4}Ca_{13.6}Cu_{24}O_{41}$ when the sample is subjected to a hydrostatic pressure of $P > 3$ GPa, above which the resistivity drops to zero at ~ 12 K. A more complex phase diagram showed that SCCO is insulating for all *x*, however it undergoes an insulator to metal transition under pressure at 7 GPa for $x = 0$ and at 3 GPa for $x > 9$. At intermediate values $1 < x < 9$ the system remains insulating at all attainable pressures (see the phase diagram in Ref. 55).

SCCO, however, exhibits all the transport signatures of a charge density wave (CDW), including a screening mode in impedance measurements [56,57], a pinning mode in microwave conductivity [58], a giant dielectric constant [56,57], and a nonlinear current–voltage (I–V) curve [56], which together indicate that the carrier density is modulated in real space. These observations are typical of conventional Peierls CDW materials like $NbSe_3$ or $K_{0.3}MoO_3$ [59] in which the carrier density is modulated by a distortion in the crystal structure, driven by the electron–lattice interaction. However a charge density wave could also be driven by effective long-range interactions such as the WC as predicted and would have the same transport signatures.

Several quite distinct studies by hard x-ray or neutron scattering showed evidence for an additional distortion of the crystal structure at low temperature [60,61,62,63,64,65]. However no other Bragg peaks than those which can be indexed according to the basic crystal structure have been observed to date as pointed out by van Smaalen [63]. In the end, there is still no direct evidence of WC in this spin ladder compound.

1.4. One-dimensional electronic system: $2k_F$ and 4 k_F instability

There are at least two general reasons for studying materials with a quasi-one-dimensional electronic structure such as SCCO. First, one-dimensional systems are often easier to handle theoretically than two- or three-dimensional systems. Secondly, characteristic low dimensional effects can be studied.

With respect to the first point, the Hubbard Hamiltonian of eq. (1.1.2) has played a crucial role. As we said above, for U<<*t*, a simple tight binding dispersion is obtained with an enhanced magnetic susceptibility [66]. For U>>*t* or large, a strongly correlated metal or Mott-Hubbard insulator is found with linear Heisenberg antiferromagnetic behavior [67].

The response of the electronic system in one dimension diverges at wave vector q = $2k_F$ where k_F is the Fermi wave vector and is equal to $\pi\rho/2c$, where *c* is the intersite spacing and ρ the number of electrons per site. This was first realized by Peierls [68]. He found that in the U = 0 limit a coupling of electrons in a regular chain to $2k_F$ phonon caused the chain to distort with that periodicity yielding a gap at the Fermi level, thereby lowering the electronic energy. Later Bani and Pincus [69] showed that in the large U limit a similar instability occurs in a one-dimensional-antiferromagnetic by modulating the exchange with wave vector $2k_F$. It was also predicted that another instability may occur at $4k_F$ [70,71]. Both $2k_F$ and $4k_F$ effects have been observed for instance in TTF-TCNQ [72] in which the charge transfer is incomplete (ρ=0.59 electrons/molecule) and hence $2k_F$ is incommensurate with lattice.

The general picture of the small-U and large-U $2k_F$ instabilities is the accommodation of two electrons per unit cell. Both limits require the possibility of having two electrons share the same orbital when their spins are antiparallel. For small U this double occupancy only costs very little Coulomb repulsion energy. When U/*t* increases the energy gained by the $2k_F$ distortion decreases, until for U → ∞ no $2k_F$ distortion will occur anymore. In ref. 73 the authors concluded that below some critical U/t value there exists a 2 k_F instability, but above it both a $2k_F$ and a 4 k_F instability can occur. The critical U/t will depend on the electron phonon coupling and in the lattice stiffness.

A $4k_F$ system with one electron per unit cell may be considered as a half-filled band which will show the usual Peierls transition to a system with two electrons per unit cell. For large U we then obtain two transitions which are (1) $4k_F$ transition thereby loosing electron-kinetic energy degrees of freedom but retaining spin entropy and (2) at lower temperature a $2k_F$ transition, doubling the unit cell to 2/ρ sites and pairing the spins. This is illustrated in **Fig. 1.4.1**. where the electron density along the chain in the three phases for ρ = ½ are plotted.

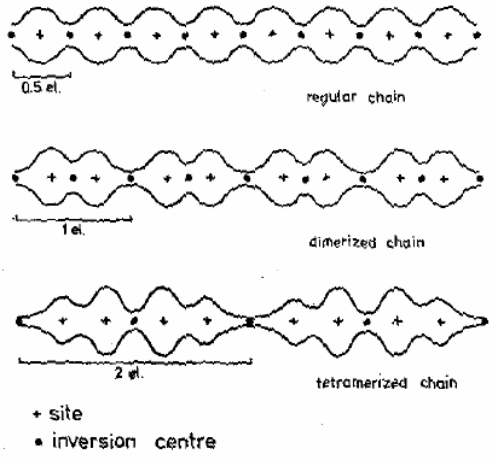

Figure 1.4.1 Schematic representation of electron densities for a quarter filled band system (ρ=1/2) in the regular chain phase (1/2 electron per unit cell), in the $4k_F$ distorted phase (1 electron per unit cell) and in the 2 k_F distorted phase (2 electrons per unit cell) [73].

The $2k_F$ transition can be called a spin Peierls transition because the transition always involves the loss of spin entropy while the $4k_F$ transition should be called an electronic Peierls transition because electronic degrees of freedom are lost. For $\rho = 0$ and $\rho = 2$ $2k_F$ and $4k_F$ are equal to reciprocal lattice vectors and no transition can occur. For $\rho = 1$ $4k_F$ equals to a reciprocal lattice vector and only the spin Peierls transition is possible. When $\rho = 2/3$ or $\rho = 4/3$ $2k_F$ differs from $4k_F$ by a reciprocal lattice vector and we can only expect one transition.

1.5. Resonant (soft) x-ray scattering (RSXS)

The most direct way to study hole crystallization or WC is x-ray scattering from which one can determine (1) its wavelength, (2) coherence length, (3) form factor (deviation from sinusoidal, for example), and (4) the temperature dependence of its order parameter, $\Delta(T)$.

It is difficult to detect a WC with hard x-ray scattering or non-resonant scattering for the following reasons. First, one needs to measure the structure factor at finite q. Second, x-ray scattering is more sensitive to structural distortions in crystals than to the charge modulation itself. The distortion in crystals can occur not only due to the charge modulation but also from other phenomena such as “misfit” between two different layers. For instance, take the case for $Sr_{14}Cu_{24}O_{41}$ (SCO). SCO is an adaptive misfit material

consisting of ladder and chain subsystems with incompatible periods c_L/c_c = 10/7. So it is very difficult to distinguish these two effects only with hard x-ray scattering.

X-ray scattering measures the square of the total electron density, $|\rho(\mathbf{q})|^2$, and the density modulation of the Wigner crystal, which arises from a small number of electrons around the Fermi level, is typically less than one electron per unit cell. In SCO, the total number of electrons contributing to allowed Bragg peaks is about 6224 (one large unit cell of SCO contains 4*(14*38+29*24+8*41) electrons). So the scattering power of a hole crystal is nominally weaker by $(1/6224)^2 \sim 10^{-8}$ for the case of only one electron contributing to the Bragg peaks which is almost impossible to detect with hard x-ray scattering.

To study such electronic ordering, we propose a new experimental method resonant soft x-ray scattering (RSXS) which is a method that is sensitive to small changes in electronic structure. RSXS is a combination of X-ray diffraction and spectroscopy in the energy range of about 200-2000 eV [see **Fig. 1.5.1**] and provides a powerful means to investigate charge ordering phenomena.

The usual x-ray scattering from an atom consists of a Thompson or "free electron" contribution, characterized by the atomic form factor f_0 = Z, as well as an anomalous contribution characterized by the anomalous form factor $f = f'+if''$. For a simple introduction to coherent scattering by multi-electron atom we follow Attwood [74]. Here, the atomic scattering amplitude is approached semi-classically based on Maxwell equations.

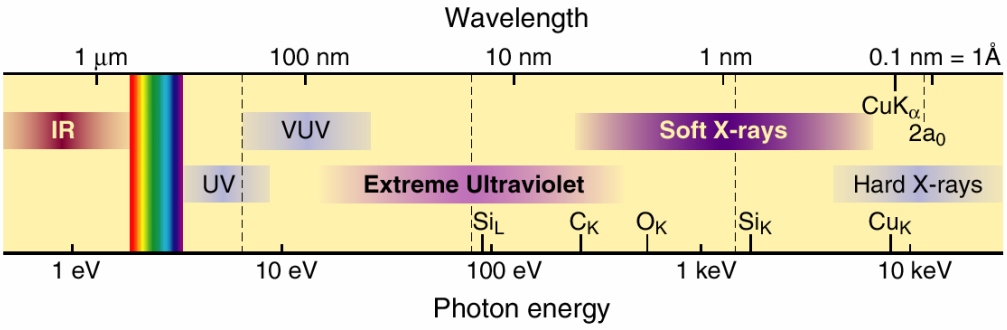

Figure 1.5.1. The short wavelength region of the electromagnetic spectrum, taken from ref. 74. Here, one can see that O *K* edge (~540 eV) and Cu $L_{2,3}$ edges (~932 eV and 952 eV) are lying in the soft X-ray range.

The photon scattering cross section is defined as the average power radiated to all angles, divided by the average incident power per unit area

$$\sigma \equiv \frac{\overline{P}_{Scatt}}{\left|\overline{\mathbf{S}}\right|} \qquad \left[Area = \frac{Power}{Power / Area} \right] \tag{1.5.1}$$

the average incident power per unit area $\overline{\mathbf{S}}$ which can be written as

$$\overline{\mathbf{S}} = \frac{1}{2}\sqrt{\frac{\varepsilon_o}{\mu_o}}\left|\mathbf{E}\right|^2 \mathbf{k}_o \tag{1.5.2}$$

where **E** is the electric field, $\mathbf{k}_o$ is propagation direction (unit vector) , while ε_o and μ_o are permittivity and permeability of free space, respectively. The average total power radiated, $\overline{P}_{Scatt}$, which is determined by integrating $\overline{\mathbf{S}}$ over the area of a distant sphere is

$$\overline{P} = \frac{1}{2}\frac{8\pi}{3}\left(\frac{e^2\left|\mathbf{a}\right|^2}{16\pi^2 \varepsilon_o c^3} \right) \tag{1.5.3}$$

where **a** is an accelerated electron and c is the velocity of light.

For a free electron the incident field causes an oscillatory motion described by Newton's second equation of motion, **F** = *m***a**, where **F** is the Lorentz force on the electron with mass *m*. By neglected $\mathbf{v}\times\mathbf{B}$ term where **v** and **B** are the velocity of the electron and magnetic field, thus the scattering cross section σ_e of an oscillating electron in which its instantaneous acceleration is $\mathbf{a}(\mathbf{r},\mathbf{t}) = -e/m\,\mathbf{E}(\mathbf{r},\mathbf{t})$ is

$$\sigma_e = \frac{8\pi}{3} r_e^2 \tag{1.5.4}$$

where r_e which is the "classical electron radius" is $r_e \equiv \frac{e^2}{4\pi\varepsilon_o mc^2}$. One can see that the scattering cross section here is independent of wavelength, and this is referred to as the Thomson cross-section for a free electron. Numerically r_e = 2.82 x 10^{-13} cm and σ_e = 6.65 x 10^{-25} cm^2. The differential Thomson scattering cross-section which is the portion of the incident energy radiated into a small solid angle in a certain direction is simply given by

$$\frac{d\sigma_e}{d\Omega} \equiv \frac{1}{\left|\mathbf{S}\right|}\frac{d\overline{P}}{d\Omega} = r_e^2 \sin^2\theta \tag{1.5.5}$$

where θ is the angle between the incident electric field vector and the direction of scattering. In terms of initial and final electric field polarization, ε_{in} and ε_{out}, the expression above becomes

$$\frac{d\sigma_e}{d\Omega} \equiv \frac{1}{\left|\mathbf{S}\right|}\frac{d\overline{P}}{d\Omega} = r_e^2 (\varepsilon_{in}^* \bullet \varepsilon_{out})^2 \tag{1.5.6}$$

For an atom with atomic number Z, the simplest approximation would be to preserve the same form, with an additional factor of Z^2 in the cross section.

For an electromagnetic wave incident upon a bound electron of resonant frequency ω_s, the force equation can be written semi-classically as

$$m\frac{d^2\mathbf{x}}{dt^2} + m\gamma\frac{d\mathbf{x}}{dt} + m\omega_s^2\mathbf{x} = -e(\mathbf{E} + \mathbf{v}\times\mathbf{B}) \tag{1.5.7}$$

with an acceleration term (*m***a**), a damping term and a restoring force term in the left hand side, and the Lorentz force exerted by the fields. For an incident electric field $\mathbf{E} = \mathbf{E}_o e^{-i\omega t}$ and neglecting the second term in the right hand side, following the same procedures used earlier, one obtains the scattering cross-section for a bound electron of resonant frequency, ω_s

$$\sigma = \frac{8\pi}{3} r_e^2 \frac{\omega^4}{(\omega^2 - \omega_s^2)^2 + (\gamma\omega)^2} \tag{1.5.8}$$

A special condition of Rayleigh scattering cross-section (1899) for a bound electron in the condition of $\omega^2 << \omega_s^2$ is $\sigma_R = \frac{8\pi}{3} r_e^2 \left(\frac{\lambda_s}{\lambda}\right)^4$ which displays a very strong λ^{-4} wavelength dependence. With this simple and elegant formula, Rayleigh explained well the blueness of the sky, the redness of the sunset and the ease of sunburning at midday.

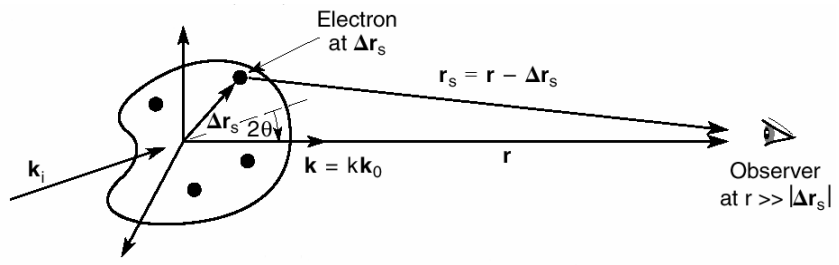

Figure 1.5.2 The scattering by multi-electron atom in semi-classical model of an atom with Z electrons and nucleus of charge +Ze at **r** = 0. $\mathbf{r}_s$ is the position of electron-*s* from center. The wave vector of incoming and out going beams are $\mathbf{k}_i$ and **k.** The detector (observer) is standing at distance **r** from the center where $\mathbf{r} >> \Delta\mathbf{r}_s$.

In reality, it is not only one electron scattered. The scattering by multi-electron atom in semi-classical model of an atom with Z electrons and nucleus of charge +Ze at **r** = 0 can be understood as follows. Assuming the distribution of electron in atom is $n(\mathbf{r},t) = \sum_{s=1}^{Z} \delta[\mathbf{r} - \Delta\mathbf{r}_s(t)]$, where $\Delta\mathbf{r}_s$ is the position of electron from center (nucleus). The wavevector of incoming and outgoing beams are $\mathbf{k}_i$ and **k.** The detector (observer) is

standing at distance **r** from the center where **r** >>|$\Delta\mathbf{r}_s$|. These are illustrated in **Fig. 1.5.2**. With this condition, the acceleration has an additional *phase* term ($\mathbf{k}_i \bullet \Delta\mathbf{r}_s$) due to the position, $\Delta\mathbf{r}_s$, within the atom:

$$\mathbf{a}_s(t) = \frac{-\omega^2}{\omega^2 - \omega_s^2 + i\gamma\omega}\frac{e}{m}\mathbf{E}_i e^{-i(\omega t - \mathbf{k}_i \bullet \Delta\mathbf{r}_s)} \tag{1.5.9}$$

The scattered electric field at a distance **r** summed for all Z electrons is

$$E(\mathbf{r},t) = \frac{-e^2}{4\pi\varepsilon_o mc^2}\sum_{s=1}^{Z}\frac{\omega^2 E_i \sin\Theta}{\omega^2 - \omega_s^2 + i\gamma\omega}\frac{1}{r_s}e^{-i[\omega(t-r_s/c)-\mathbf{k}_i \bullet \Delta\mathbf{r}_s]} \tag{1.5.10}$$

where $\mathbf{r}_s \equiv \mathbf{r} - \Delta\mathbf{r}_s$ and $r_s = |\mathbf{r}_s|$, while Θ is an angle between the direction of acceleration **a** and the observation direction $\mathbf{k}_o$. For r >> $\Delta\mathbf{r}_s$ in which $r_s \approx r - \mathbf{k}_o \bullet \Delta\mathbf{r}_s$, then eq. (1.5.10) simplifies to $E(\mathbf{r},t) = \frac{-r_e}{r} f(\Delta\mathbf{k},\omega)E_o \sin\Theta\, e^{-i\omega(t-r_s/c)}$ where $f(\Delta\mathbf{k} = \mathbf{k} - \mathbf{k}_i, \omega)$ is defined as

$$f(\Delta\mathbf{k},\omega) \equiv \sum_{s=1}^{Z}\frac{\omega^2 e^{-i\Delta\mathbf{k}\bullet\Delta\mathbf{r}_s}}{\omega^2 - \omega_s^2 + i\gamma\omega} \tag{1.5.11}$$

Here ($\Delta\mathbf{k} \bullet \Delta\mathbf{r}_s$) is a phase term. The quantity $f(\Delta\mathbf{k}, \omega)$ is the complex atomic scattering factor (f_1+*i* f_2), which tells us the scattered electric field due to a multi-electron atom. In x-ray scattering experiments the form factors are related to the absorptive part of the index of refraction by $Im[n(\Delta\mathbf{k},\omega)] = -\, r_e\lambda^2/2\pi\, V_{cell}\ Im[\ \Sigma_i\ f_i\ (\Delta\mathbf{k},\omega)\ ]$, where λ is the x-ray wavelength. The real part of the atomic scattering factor is related to the imaginary part by the Kramers-Kronig dispersion relation [75]:

$$f_1 = Z - (Z/82.5)^{2.37} + \frac{2}{\pi\hbar c}\int_0^\infty \frac{\varepsilon^2\lambda}{E^2 - \varepsilon^2}d\varepsilon \tag{1.5.12}$$

In general the ($\Delta\mathbf{k} \bullet \Delta\mathbf{r}_s$) phase terms do not simplify, but in two cases they do. The conditions where the atomic scattering factor $f(\Delta\mathbf{k}, \omega)$ simplifies significantly are

$|\Delta\mathbf{k} \bullet \Delta\mathbf{r}_s| \to 0$ for $a_o/\lambda << 1$ (long wavelength limit) (1.5.12a)

$|\Delta\mathbf{k} \bullet \Delta\mathbf{r}_s| \to 0$ for $\theta << 1$ (forward scattering) (1.5.12b)

In each of these two cases the atomic scattering factor $f(\Delta\mathbf{k}, \omega)$ reduces to

$$f^o(\omega) = f_1 + if_2 = \sum_{s=1}^{Z}\frac{\omega^2}{\omega^2 - \omega_s^2 + i\gamma\omega} = \sum_s \frac{g_s\omega^2}{\omega^2 - \omega_s^2 + i\gamma\omega} \tag{1.5.13}$$

where g_s which is oscillator strengths is associated with each resonance and normalized by the condition $\sum_s g_s = Z$.

Here, we give one example of Oxygen scattering factor [see **Fig. 1.5.3**]. From eq. (1.5.13), one can see that for $\hbar\omega >> \hbar\omega_s$, $f_1^o \to Z$. This works here for Oxygen $f_1^o \to 8$, but note that in general this conflicts with the condition λ >> a_0 (a_0 = 0.529 Å which is Bohr

radius). For the case of Oxygen at 4 Å wavelength ($\lambda >> a_0$), and thus $\hbar\omega$ = 3 keV ($>>\hbar\omega_s$~540 eV), the atomic scattering cross-section is $\sigma(\omega) = (8\pi/3)\, r_e^2 \left| f_o(\omega) \right|^2 \approx Z^2 \sigma_e$ that is, all Z electrons are scattering cooperatively (in-phase) - the so-called N^2 effect. Of course, in resonance condition ($\hbar\omega_s$ ~ 540 eV), there is no guarantee that the phase effect can be neglected.

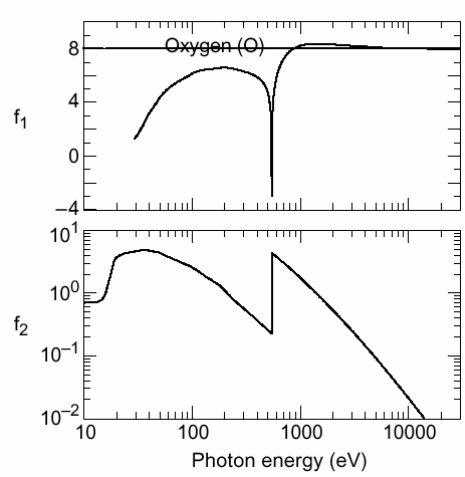

Figure 1.5.3 Oxygen scattering factor from ref.75.

The derivation of atomic scattering amplitude using a quantum field theory approach can be found in the books of Sakurai [76] or also can be found in books of Blume in ref. 77.

In x-ray scattering experiments, one can tune the incoming photon energy and its polarization to an absorption transition of a selected atom, so that the scattering cross-section of this particular atom and orbital is greatly enhanced through a resonant scattering process [77]. Usually, resonant scattering is conducted in the hard x-ray regime, for example, using a deep core to valence transition of a heavy atom [78]. However, in many strongly correlated materials, Oxygen *2p* and transition metal *3d* orbitals determine the low energy behavior and their fascinating properties. Resonant hard x-ray scattering, based on Cu *1s→4p* for example, probes the local density of the empty *4p* states and is an indirect and relatively insensitive probe for what is happening in the *3d* orbitals. The interpretation of resonant hard x-ray scattering data of these materials is often controversial and complicated [79,80]. To go beyond hard x-ray experiments, one should perform resonant scattering based on *O1s→2p* (~530 eV), or transition metal *2p→3d* transitions (~930 eV). Note here that, the wavelength of the photon with energy range of 500 to 900 eV is about

20 to 12 Å. This range of the wavelength is well matched to the charge or spin orderings which occur in strongly correlated systems, such as "stripes" in LBCO, the "checkerboard" Wigner crystal in $Ca_{2-x}Na_xCuO_2Cl_2$ [81], quasiparticle interference in $Bi_2Sr_2CaCu_2O_{8+\delta}$ [82,83,84], etc., which have periodicities of order 10-20 Å.

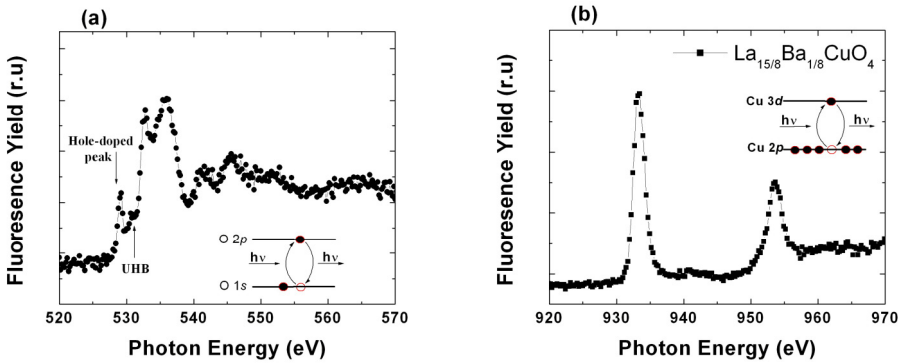

Figure 1.5.4 X-ray absorption spectrum taken in Fluorescence Yield mode for (**a**) O 1*s* to 2*p* transitions (**b**) Cu 2*p* to 3*d* transitions in $La_{15/8}Ba_{1/8}CuO_4$. The inset illustrates (a) O 1*s*→2*p* (b) Cu 2*p*→3*d* resonant scattering.

As illustrated in **Fig. 1.5.4**, when the photon energy is tuned to (**a**) the *O1s→2p* (~530 eV) or (**b**) transition metal *2p→3d* transitions (~930 eV), the contribution from (a) O or (b) Cu atoms to the scattering is greatly enhanced through a virtual excitation process called resonant or anomalous scattering [77]. In the dipole approximation, it is described by the atomic form factor:

$$f \propto \sum_f \left| \sum_m \frac{\langle \psi_f, \omega_1 | \vec{\varepsilon} \bullet \vec{r} | \psi_m \rangle \langle \psi_m | \vec{\varepsilon}' \bullet \vec{r} | \psi_f, \omega_1 \rangle}{E_m - E_i - \hbar\omega_o - i\Gamma_m} \right| \delta\left(E_f - \hbar\omega_1 - E_i - \hbar\omega_o\right) \quad (1.5.14)$$

where Ψ_i, Ψ_m, and Ψ_f are the initial, intermediate, and final state wavefunctions with energies of E_i, E_m, and E_f respectively. Γ_m is the lifetime energy broadening of the intermediate state. ω_0 and ω_1 are the incoming and scattered photons with polarization ε and ε' respectively. Resonant elastic scattering as we are interested in here occurs when the system returns to the ground state so the final and the initial states of the system are the same. In this case the scattering signal contains information of electronic structure of the states involved. If ψ_i contains 2*p* or 3*d* holes, *O1s→2p* or *2p→3d* is allowed to the state ψ_m, and therefore the O 2*p* or Cu 3*d* state and their spatial distribution are probed directly. On the contrary, ordinary resonant hard x-ray scattering based on Cu 1*s*→4*p* transition only probes empty 4*p* states, which contribute only weakly to the low energy physics in the problem.

The *O1s→2p* and Cu *2p→3d* transition have been extensively studied by x-ray absorption spectroscopy (XAS) [85,86,87,88,89]. The O *K* edge shows a "pre-peak" feature (~531 eV) that is an intersite O 1*s* → Cu 3*d* transition [90] brought about by *p-d* hybridization [see **Fig. 1.4.1**(**a**)]. This feature is well-known as the Upper Hubbard Band (UHB). When the system is doped, added holes go into O 2*p* states [90] and a second prepeak, which is the doped hole peak, appears at ~529 eV. Its oscillator strength builds rapidly with hole concentration as states near the Fermi level are vacated and also as spectral weight is transferred to 529 eV from the feature at 531 eV [90]. A transfer of spectral weight with doping is the classic signature of correlated system [91], and it makes the optical response at 529 eV extremely sensitive to the local hole density. Because the valence states are polarized in the CuO_2 plane, both the oxygen prepeak and the doped hole features are observable in XAS only when E||*ab* [85]. The Cu *L* edge is better described as a peak rather than an edge and it consist of two peaks, due to spin orbit coupling of the core levels, corresponding to the dipole-allowed *2p→3d* transitions where the hole has *j* = 1/2 or 3/2 [see **Fig. 1.4.1** (**b**)] [85]. Because the unoccupied Cu 3*d* states in the high T_c's are $d_{x^2-y^2}$ states they are polarized in the CuO_2 plane, and the Cu *L* feature is observable in XAS only for E||*ab* [86].

1.6. Scope

As we discussed above, here we investigate the existence of hole crystallization or Wigner crystallization in Cu-O systems with a new experimental method called RSXS. During this study, a UHV-diffractometer was developed. RSXS measurements were done on the soft x-ray undulator line X1B at the National Synchrotron Light Source (NSLS) in Brookhaven National Laboratory (BNL).

The manuscript is organized as follows. In Chapter 2, we describe the beamline X1B and the UHV-diffractometer. In Chapter 3, we report tests of the RSXS technique on a few important materials, such as thin films of La_2CuO_4, single crystals of ortho-II YBCO, and a single crystal of $Bi_2Sr_2CaCu_2O_{8+\delta}$. Chapter 4 shows the first direct evidence of the WC in ladders and a $4k_f$ CDW in the chains of $Sr_{14}Cu_{24}O_{41}$. Chapter 5 contains a new interpretation of polarization-dependent X-Ray Absorption from the spin ladder of $Sr_{14-x}Ca_xCu_{24}O_{41}$. In chapter 6, we show the importance of commensurability to the stability of WC on a lattice in ladders and hole pinning mechanism in chains of spin ladder of $Sr_{14-x}Ca_xCu_{24}O_{41}$. And in the chapter 7, we present our study of charge character of the static 'stripe' phase in $La_{15/8}Ba_{1/8}CuO_4$.

References

[1] F. Bloch, *Z. Phys*. **57**, 545 (1929).

[2] A. H. Wilson, *Proc. Roy. Soc. A* **133**, 458 (1931).

[3] H. J. De Boer and E. J. W. Verwey, *Proc. Phys. Soc. A* **49**, 59 (1937).

[4] N. F. Mott and R. Peierls, *Proc. Phys. Soc. London, Sect. A* **49**, 72 (1937).

[5] N. F. Mott, Proc. *Phys. Soc. London, Sect A* **62**, 416 (1949).

[6] N. F. Mott, Can. *J. Phys.* **34**, 1356 (1956).

[7] N. F. Mott, *Philos. Mag.* **6**, 287 (1961).

[8] J. Hubbard, *Proc. R. London Soc., Ser A* **277**, 237 (1964).

[9] J. Hubbard, *Proc. R. London Soc., Ser A* 281, 401 (1964).

[10] P. W. Anderson, *Phys. Rev.* **115**, 2 (1959); *Solid State Physics* **14**, 99 (1963).

[11] J. Kondo, *Prog. Theoret. Phys.* **28**, 846 (1962); **32** 37 (1964); **34** 204 (1965).

[12] M. B. Brodsky in "Valence Instabilities and Related Narrow Band Phenomena", edited by R. D. Parks (Plenum, New York, 1977), p. 351.

[13] P. W. Anderson, *Phys. Rev.* **124**, 41 (1961).

[14] For a review, "Electron Correlation and Magnetism", Patrik Fazekas (World Scientific 1999).

[15] P. Hohenberg and W. Kohn, *Phys. Rev. B* **136** 864 (1964); W. Kohn and L. J. Sham, *Phys. Rev. A* **140** 1133 (1964).

[16] "Theory of the Inhomogeneous Electron Gas", edited by S. Lundqvist and N. H. March (Plenum, 1983); G. D. Mahan and K. R. Subbaswamy, "Local Density Theory of Polarizability", (Plenum, 1990).

[17] Vladimir I. Anisimov et al., *Phys. Rev. B* **44** 943 (1991).

[18] C.M. Varma, et al., *Phys. Rev. Lett.* **63**, 1996 (1989); **64**, 497 (1990).

[19] D. Pines, in "High Temperature Superconductivity" edited by K. S. Bedell, *et al.*, p. 392, Addison Wesley, New York (1990).

[20] J. B. Torrance et al., *Phys. Rev B* **15**, 4738 (1977).

[21] D. J. Klein, W. A. Seitz, *Phys. Rev B* **10**, 3217 (1974).

[22] Brinkman & Rice. *Phys. Rev. B* **2**, 1324 (1970).

[23] P. W. Anderson, *Science* **235**, 1196 (1987).

[24] For a review, J. Orenstein and A. J. Millis, *Science* **288**, 468 (2000).

[25] J. Zaanen, G. A. Sawatzky, and J. W. Allen, *Phys. Rev. Lett.* **55**, 418 (1985).

[26] A. Bocquet, T. Mizokawa, T. Saitoh, H. Namatame, and A. Fujimori, *Phys. Rev. B* **46**, 3771 (1992)

[27] J. G. Bednorz and K. A. Müler, *Z. Phys. B* **64**, 189 (1986).

[28] C. M. Varma, *Phys. Rev. Lett.* **83**, 3538 (1999).

[29] C. M. Varma, *Phys. Rev. B* **55**, 14554 (1997).

[30] F. C. Zhang and T. M. Rice, *Phys. Rev. B* **37**, 3759 (1988).
[31] D. Wollman, et al., *Phys. Rev. Lett.* **71**, 2134 (1993).
[32] C. C. Tsuei, et al., *Phys. Rev. Lett.* **73**, 593 (1994).
[33] J. R. Kirtley, et al., *Nature* **373**, 225 (1995).
[34] C. C. Tsuei, et al., *Science* **272**, 329 (1996).
[35] M. N. Maple, *J. Mag. Mag. Mat.* **18**, 177-181(1998).
[36] K. Machida, *Physica C* **158**, 192-196 (1989).
[37] J. Zaanen & O. Gunnarsson, *Phys. Rev. B* **40**, R7391-R7394 (1989).
[38] H. J. Schulz, *Phys. Rev. Lett.* **64,** 1445–1448 (1990).
[39] S. A. Kivelson & V. J. Emery, in *Strongly Correlated Electron Materials: The Los Alamos Symposium1993* (eds Bedell, K. S., Wang, Z., Meltzer, D. E., Balatsky, A. V. & Abrahams, E.) 619–650 (Addison-Wesley, Redwood City, 1994).
[40] C. Nayak & F. Wilczek, Populated domain walls. *Phys. Rev. Lett.* **78,** 2465–2468 (1997).
[41] A. H. Castro-Neto, *Phys. Rev. Lett.* **78,** 3931–3934 (1997).
[42] Devreese, J. T., Evrard, R. P. & van Doren, V. E. (eds) *Highly Conducting One-Dimensional Solids* (Plenum, New York, 1979).
[43] S. A. Kivelson, E. Fradkin & V. J. Emery, *Nature* **292**, 550 (2004).
[44] P. W. Anderson, *Science* **235**, 1196 (1987).
[45] P. Lee, *Physica* C **194**, 317-318 (1999).
[46] Y. Noda & M. Imada, *Phys. Rev. Lett.*, **89**, 176803 (2002).
[47] J. M. Tranquada, B. J. Sternlieb, J. D. Axe, Y. Nakamura, & S. Uchida, *Nature*, **375**, 561-563 (1995).
[48] M. Fujita, H. Goka, K. Yamada, M. Matsuda, *Phys. Rev. Lett.*, **88**, 167008 (2002).
[49] J. M. Tranquada, J. D. Axe, N. Ichikawa, Y. Nakamura, S. Uchida, B. Nachumi, *Phys. Rev. B*, **54**, 7489-7499 (1996).
[50] A. R. Moodenbaugh *et al*., *Phys. Rev. B*, **38**, 4596-4600 (1988).
[51] E. Dagotto, J. Riera, D. Scalapino, *Phys. Rev. B*, **45**, 5744 (1992).
[52] M. Siegrist, T. M. Rice, and F. C. Zhang, *Phys. Rev. B*, **65**, 165122 (1994).
[53] S. T. Carr, & A. M. Tsvelik, *Phys. Rev. B* **65**, 195121 (2002).
[54] S. R. White, I. Affleck, & D. J. Scalapino, *Phys. Rev. B* **65**, 165122 (2002).
[55] K. M. Kojima, N. Motoyama, H. Eisaki, S. Uchida, *J. Elect. Spect. Rel. Phen.*, **117**, 237 (2001).
[56] G. Blumberg *et al*., *Science* **297**, 584–587 (2002).
[57] B. Gorshunov *et al*., *Phys. Rev. B* **66**, 60508(R) (2002).
[58] H. Kitano *et al*., *Europhys. Lett.* **56**, 434–440 (2001).
[59] G. Grüner, *Density Waves in Solids* (Perseus, Cambridge, MA, 1994).
[60] M. Matsuda, T. Yosihama, K. Kakurai, G. Shirane, *Phys. Rev. B* **59**, 1060 (1999).

[61] D. E. Cox, T. Iglesias, K. Hirota, G. Shirane, M. Matsuda, N. Motoyama, H. Eisaki, S. Uchida, *Phys. Rev. B* **57**, 10750 (1998).
[62] T. Fukuda, J. Mizuki, M. Matsuda, *Phys. Rev. B* **66**, 12104 (2002).
[63] S. van Smaalen, *Phys. Rev. B*, **67**, 26101 (2003).
[64] J. Etrillard, M. Braden, A. Gukasov, U. Ammerahl, A. Revcolevschi, *Physica C*, **403**, 290 (2004).
[65] M. v. Zimmermann, *et al.*, cond-mat/0406215.
[66] J. B. Torrance et al., *Phys. Rev B* **15**, 4738 (1977).
[67] D. J. Klein, W. A. Seitz, *Phys. Rev B* **10**, 3217 (1974).
[68] R. E. Peierls, Quantum Theory of solids (Oxford University, London, 1955).
[69] G. Beni and P. Pincus, *J. Chem. Phys*. **57**, 3531 (1972).
[70] J. B. Torrance in " Chemistry and Physics of one-dimensional metals" edited by H.J. Keller, 137 (1977) and references therein.
[71] M. Weger, H. Gutfreund, *Sol. St. Comm.* **32**, 1259 (1979).
[72] S. Kagoshima et al., *J. Phys. Soc. Jpn.* **41,** 2061 (1976); J. P. Pouget et al**,** *Phys. Rev. lett.* **37,** 437 (1976).
[73] S. Huizinga, *et al.*, *Phys. Rev. B* **19**, 4723–4732 (1979).
[74] David T. Attwood, *Soft X-Rays and Extreme Ultraviolet Radiation:Principles and Applications*, (Cambridge University).
[75] B. L. Henke, E. M. Gullikson, & J. C. Davis, X-ray interactions: photoabsorption, scattering, transmission, and reflection at *E*=50-30000 eV, Z=1-92, *Atomic Data and Nuclear Data Tables*, **54**, 181-342 (1993).
[76] J. J. Sakurai, *Advanced Quantum Mechanics*, (Addison-Wesley).
[77] M. Blume, M. in *Resonant Anomalous X-Ray Scattering* (eds. Materlik, G. *et al.*) 495-512 (North-Holland, Amsterdam, 1994).
[78] Y. Murakami *et al*, *Phys. Rev. Lett.* **82**, 1932-1935 (1998).
[79] Ishihara, S. & Maekawa, S. *Phys. Rev. Lett.* **80**, 3799-3802 (1998).
[80] I. S. Elfimov *et al*,, *Phys. Rev. Lett.* **82**, 4264-4267 (1999).
[81] T. A. Hanaguri *et al.*, *Nature*, **430**, 1001 (2004).
[82] K. McElroy et al., *Phys. Rev. Lett* .**94,** 197005 (2005).
[83] J.E. Hoffman et al., *Science* **297**, 1148 (2002).
[84] Michael Vershinin *et al.*, *Science* **303**, 1995 (2004).
[85] C. T. Chen *et al*., *Phys.Rev.Lett*. **66,** 104 (1991).
[86] C. T. Chen *et al*., *Phys. Rev. Lett*. **68,** 2543 (1992).
[87] N. Nücker *et. al.*, *Phys. Rev. B*, **62**, 14384-14392 (2000).
[88] N. Nücker *et. al.*, *Phys. Rev. B*, **39**, 6619 (1989).
[89] F. J. Himpsel *et. al.*, *Phys. Rev. B*, **38**, 11946 (1988).
[90] F. C. Zhang, T. M. Rice, *Phys. Rev. B* **37,** R3759 (1988).

[91] H. Eskes, M. B. J. Meinders, G. A. Sawatzky, *Phys. Rev. Lett.* **67,** 1035 (1991).

I will first focus on Cu L-edge resonant scattering experiments that led us to uncover charge density wave (CDW) correlations, in the absence of magnetic field, competing with superconductivity in the YBCO family1-3. A complete temperature and doping dependent phase diagram has been worked out4. These investigations have been extended to other families of cuprates (Bi22015, Bi22126 and Hg12017) demonstrating the ubiquity and the universality of the phenomenon. Further information was gained from high resolution inelastic x-ray scattering. The observation of a quasi-elastic â€˜central peakâ€™ unrav Resonant inelastic soft X-ray scattering in quasi one dimensional cuprates. Determining crystal-field excitations in heavy fermion materials with x-rays. Inelastic soft X-ray scattering of protein and amino acids in water.Â Intra-site electronic correlations in polarization-resolved resonant inelastic soft X-ray scattering. RIXS study on high-Tc cuprates and related compounds.Â Among others the chains develop a charge density wave at low temperatures, whereas the ladders possess a quantum mechanical spin liquid ground state with a finite spin gap [3]. With Cu L3-RIXS we map out the dispersion of two-triplon excitations, the elementary magnetic excitations in the ladders, achieving excellent sensitivity over almost the full Brillouin-zone and directly determining the. 2.2 Resonant X-rays scattering. In diffraction or in absorption techniques an incoming photon is absorbed and a core electron is promoted to an empty continuum state or an empty bound state, depending on the photon energy.Â The charge scattering does not change the scattered x-ray polarization and the x-ray intensity is detected only when = 0â—¦, i.e. in the âˆ’ polarization channel. b) X-ray diffraction of a magnetic reection Q = (0, 0, 2.5). The magnetic moments are oriented perpendicular to the scattering plane when the azimuthal angle = 0â—¦. Both polarization channels âˆ’ (open circles) and âˆ’.Â This scattering conguration is particularly useful in the determination of the magnetic moment orientation or the magnetic S-domain population.